ISSN 1573-160X, *PHYSICAL OCEANOGRAPHY*, Vol. 33, Iss. 4, pp. 565-583 (2026)
Original Russian Text © The Authors, 2026,
published in *Morskoy Gidrofizicheskiy Zhurnal*, 2026, Vol. 42, Iss. 4, pp. 536–555

Original article

Impact of the Langmuir Circulations on Vertical Turbulent Exchange in the Sea Wave Layer

M. I. Pavlov ✉, A. M. Chukharev, D. V. Kazakov, A. G. Zubov, O. I. Pavlenko, S. A. Shutov

Marine Hydrophysical Institute of RAS, Sevastopol, Russian Federation
✉ *mixail.pavlov.1993@mail.ru*

Abstract
Purpose. The purpose of the study is to parameterize the Langmuir circulation based on experimental data on the main hydrophysical parameters, to determine the relationship between its characteristics and surface waves, and to assess the impact of coherent structures on vertical turbulent exchange in the wave-enhanced surface layer.
Methods and Results. During 2021–2024, hydrophysical fields near the sea surface, including their fluctuation characteristics, were comprehensively measured at the stationary oceanographic platform (Katsiveli) using the acoustic Doppler current profilers (ADCP) DVS-6000 and Workhorse Monitor 1200, as well as a Sigma-1 turbulence meter and a meteorological complex. The vertical velocity component W in the convergence zones was identified at 3–4 m depth based on the ADCP data. The measured values of W allowed the dependences of the Langmuir circulation parameters on wind speed at a height of 10 m (V_{10}) to be determined. To distinguish the modes, the Gaussian mixture model clustering method was applied; it included the selection of the number of clusters based on the Bayesian information criterion. The rate of turbulent kinetic energy dissipation ε was calculated from the velocity fluctuation spectra. Two modes – energy-dependent ($La_t > 0.98$) and saturated ($La_t \leq 0.98$) – were distinguished. The regression relationships $W_1 = 0.57V_{10} + 1.15$ ($R^2 = 0.52$) and $W_2 = = 0.29V_{10} + 7.3$ ($R^2 = 0.51$) were obtained for these modes. The median values of the Langmuir number La_t were 1.2 (IQR = 0.53) and 0.8 (IQR = 0.34) for the energy-dependent and saturated modes, respectively. It was found that the median values of ε in both modes were close ($2.87 \cdot 10^{-6}$ and $2.62 \cdot 10^{-6}$ m²/s³), but the IQR of log10(ε) in the energy-dependent mode (0.75) exceeded that in the saturated mode (0.40) by a factor of 1.9. This indicated a significant difference in turbulence variability.
Conclusions. The effect of Langmuir circulation on vertical turbulent exchange lies not so much in altering the mean dissipation rate as in modulating the variability regime, namely, in the transition from a chaotic and inhomogeneous state to an organized and statistically homogeneous one. The proposed parameterizations of $W(V_{10})$ and quantitative estimates of ε can be used to improve models of turbulence in the wave-enhanced surface layer.

Keywords: vertical turbulent exchange, sea wave layer, dissipation rate, Stokes drift, experimental studies, Langmuir circulation, turbulent Langmuir number, Black Sea hydrophysical subsatellite polygon, stationary oceanographic platform

Acknowledgements: The study was carried out within the framework of the state assignment of FSBSI FRC MHI, No. FNNN-2024-0001.

For citation: Pavlov, M.I., Chukharev, A.M., Kazakov, D.V., Zubov, A.G., Pavlenko, O.I. and Shutov, S.A., 2026. Impact of the Langmuir Circulations on Vertical Turbulent Exchange in the Sea Wave Layer. *Physical Oceanography*, 33(4), pp. 565-583.

Introduction

The atmospheric surface layer and the ocean surface layer are parts of the boundary layers directly adjacent to the interface between the media. Their dynamics are critically important for the formation of turbulent mixing. Turbulence developing in the ocean surface layer determines the intensity of vertical turbulent exchange and, consequently, exerts a key influence on the transfer of heat, momentum, and gases across the ocean–atmosphere interface.

Turbulent mixing depends on background physical conditions and on motions of various scales; therefore, studying this phenomenon and its fundamental patterns requires investigating other processes that determine its intensity and variability.

The main factors modulating turbulence in the sea surface layer are considered to be the shear in the drift-current velocity, instability of surface-wave-induced motions, and surface-wave breaking [1]. Turbulence intensity in the sea surface layer is well predicted by widely known models [1–3] at wind speeds measured at 10-m height above the sea surface (V_{10}) ranging from 5 to 9 m/s. Under stronger winds and storm conditions, the best agreement between the calculated and experimental results is demonstrated by the stationary multiscale model developed by A.M. Chukharev at the Turbulence Department of Marine Hydrophysical Institute [3]. Model calculations for weak winds and weak wave conditions are substantially lower than the experimental values: discrepancies can reach 2–3 orders of magnitude. Several studies [4–9] have suggested that this may be related to the influence of Langmuir circulation (LC), which is not accounted for in these models. Langmuir circulation consists of pairs of alternating cylindrical vortices rotating in opposite directions around parallel horizontal axes oriented approximately normal to the wind-wave fronts. Foam bands or floating debris streaks on the water surface are commonly used as indicators of LC. Characteristic features of Langmuir bands include their appearance at certain wind speeds, alignment with the wind direction, quasi-regular spacing, and widespread occurrence, as well as rapid reorientation in response to wind direction changes. At the water surface, LC is identified at scales ranging from 2 m to 1 km.

In prognostic models, LC is mainly represented using large-eddy simulation (LES) [10–12], in which Stokes drift serves as an important parameter for calculating the turbulent Langmuir number La_t. Model simulations cover spatial scales from 1 m to 10 km (so-called submesoscales). Various issues are studied, such as the influence of swell on LC formation, the structure of LC following the passage of a cyclone, and the rate of pycnocline erosion. In [5], large-scale experiments were conducted, and the main characteristics of LC identified using various methods were described. A formula was proposed for calculating LC intensity based on the water friction velocity and Stokes drift. Subsequently, most researchers began using the same parameters for both qualitative and quantitative analyses of LC characteristics.

---

[1] Monin, A.S. and Ozmidov, R.V., 1981. *Oceanic Turbulence*. Leningrad: Gidrometeoizdat, 320 p. (in Russian).

LES models successfully reproduce many observed LC features, particularly instability, the non-uniform size distribution of cells, their merging through Y-shaped transitions oriented downwind, and the alignment of floating particles into linear bands [13]. LC enhances turbulent mixing near the surface; however, existing LES models do not account for its relationship with surface waves and wave breaking. Compared with field data at low wind speeds, LES modeling overestimates the TKE dissipation rate.

Experimental studies [14, 15] have yielded numerous results describing the influence of LC on vertical turbulent exchange. One of the main conclusions is that LC not only generates turbulence but also transports water containing air bubbles formed during wave breaking, thereby deepening the mixed layer. Field measurements in Chesapeake Bay [16] confirmed the important role of LC in the dynamics of the surface layer as a whole. However, relating LC parameters to physical quantities characterising near-surface turbulence is a non-trivial task. Approximate parameterisations of vertical velocity in convergence zones as a function of wind speed were presented in [17, 18]. However, the sensitivity and accuracy of the instruments used were insufficient to obtain reliable results; therefore, the demonstrated scatter in the data points is difficult to describe using the proposed relationships.

In [19], the following parameterisations were tested to account for the influence of LC on turbulent exchange in the multiscale turbulence model [3]:

$$P^L = \nu_t \left(\frac{\partial U}{\partial z} \frac{\partial U_s}{\partial z} + \frac{\partial V}{\partial z} \frac{\partial V_s}{\partial z} \right), \tag{1}$$

where U, V, U_S, V_S are the components of mean current velocity and the Stokes drift along the horizontal x- and y-axes, respectively; ν_t is the turbulent viscosity [20];

$$\frac{< w'^2 >}{u_*^2} = \begin{cases} 0{,}398 + 0{,}48 La_{SL}^{-4/3}, & La_{SL} \le 1, \\ 0{,}64 + 3{,}50 \exp(-2{,}69 La_{SL}), & La_{SL} > 1, \end{cases} \tag{2}$$

where $< w'^2 >$ is the root-mean-square vertical current velocity fluctuations; u_* is the water friction velocity; La_{SL} is the turbulent Langmuir number calculated from the Stokes drift averaged over the upper 1/5 of the mixed layer [21].

Model simulations showed that when parameterization (1) was used, the influence of LC on turbulence intensity was negligible (less than 1%). Relationship (2) makes a negligible contribution when $La_t > 1$, but when $La_t < 1$, its influence increases noticeably (up to 15% at $La_t = 0.63$). Unfortunately, these results do not provide a clear picture of the LC effect on turbulent exchange in the surface layer.

This study aims to develop a parameterization of LC based on experimental data obtained at the stationary oceanographic platform (SOP) of the Black Sea Hydrophysical Subsatellite Polygon (BSHSP) at Katsiveli during 2019–2024, determine the relationship between its characteristics and surface waves, and quantitatively assess the influence of these coherent structures on vertical turbulent exchange in the wave-enhanced surface layer.

In this study, we relied on the Craik–Leibovich theory [4] of the emergence of LC through the interaction between Stokes drift induced by surface waves and vertical velocity shear in a turbulent fluid, which generates a vortex force. This study continues our previous research on turbulence in the upper-ocean boundary layer (2021–2024) and develops theoretical and modeling concepts based on a more reliable parameterization of an important source of turbulence.

Materials and methods

During 2021–2024, experimental studies of LC were carried out at the SOP in Katsiveli. The aim of the work was to determine the relationship between LC parameters and the parameters of wind and surface waves, as well as to assess the influence of LC on vertical turbulent exchange. Based on [14–23], the vertical component of the current velocity, W, in convergence and divergence zones was chosen as the main parameter characterizing the dynamics of LC. Based on [14, 23], we developed a method for determining W within Langmuir coherent structures using acoustic Doppler current profilers (ADCPs).

The DVS-6000 and Workhorse Monitor 1200 systems were used; they were installed at 5 and 2 m depth, respectively (Fig. 1). The DVS-6000 transducers were directed upward; measurements were carried out over the depth range of 0.4–4.5 m in five 0.8-m-thick layers (bins); the velocity values were referenced to the centre of each layer. The instrument was set to 50 pings per minute, with a current velocity resolution of 0.24 cm/s. The instrument was placed in a special frame and weighted down to minimize its movement and improve measurement accuracy.

The Workhorse Monitor 1200 was mounted on a boom rigidly attached to the SOP structure. The transducers of this instrument were directed downward. Measurements were carried out over the depth range of 3–8 m in five 1-m-thick layers (bins); the velocity values were referenced to the centre of each layer. The instrument was also set to 50 pings per minute. The current velocity resolution was 0.3 cm/s.

The Vostok-M measurement system was located at a depth of 3 m and recorded the mean values of current velocity, electrical conductivity, and temperature. To assess the intensity of turbulent processes and the influence of LC on vertical mixing, the three fluctuating components of the velocity vector (u', v', w') were measured at depths of 2–4 m using the Sigma-1 system developed at Marine Hydrophysical Institute [24]. The MPV 702.10007 meteorological system was used to record wind speed V_{10} and other meteorological parameters. A more detailed description of the instrument arrangement is given in study [25]. The locations of ADCP systems, the arrangement of instruments in the working area on the seaward side of the SOP, and a schematic representation of the experimental setup are shown in Figs. 1 and 2.

The measurement procedure was as follows: to assess the influence of LC on vertical turbulent exchange in the wave-enhanced surface layer (the reference measurement depth was approximately 3 m), the following parameters were recorded for periods of 3–10 h: W, u', v', w', V_{10}, and the mean values of current velocity, electrical conductivity, and temperature. Surface wave parameters were determined by the staff of the Remote Sensing Department of MHI and provided for analysis.

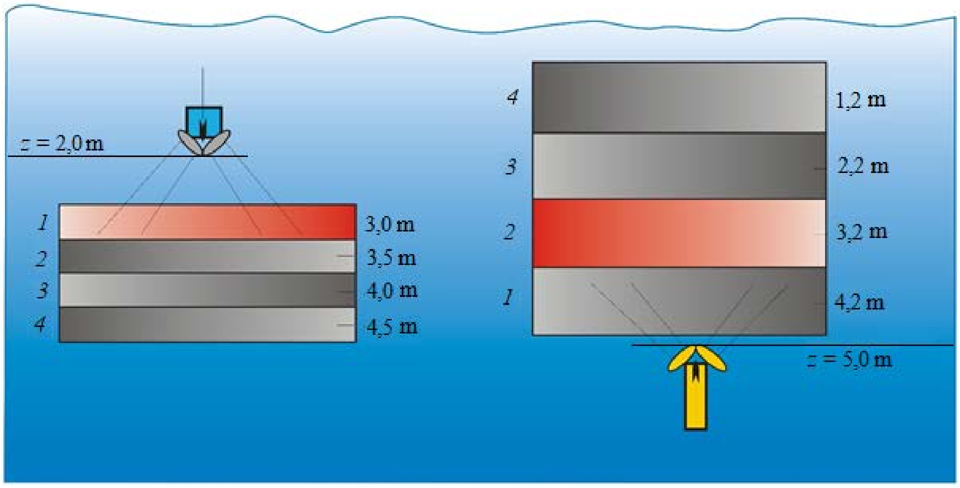

F i g. 1. Diagram of installation of the ADCP Workhorse 1200 (*left*) and DVS-6000 (*right*) measuring systems. Main horizon for measuring the LC parameters is highlighted in red. Numerals *1*–*4* indicate the ordinal numbers of layers; *z* is the instrument installation depth

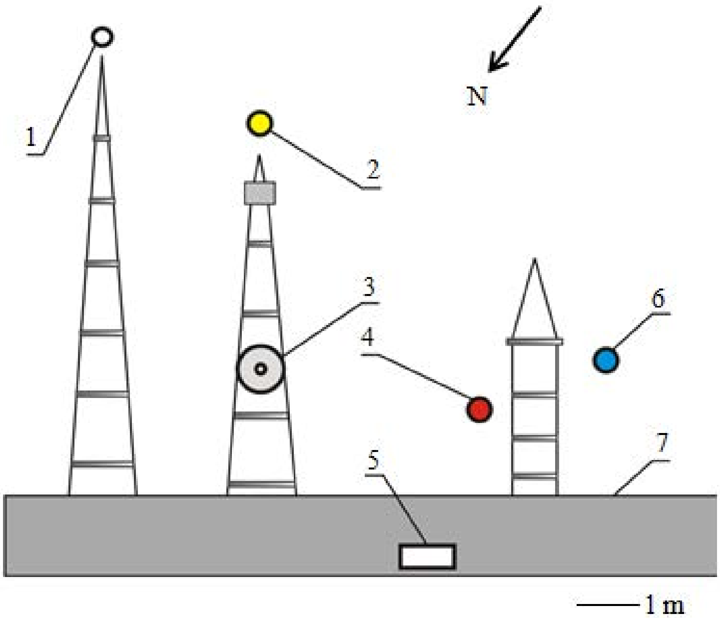

F i g. 2. Diagram of instrument arrangements during the expedition on the oceanographic platform at the BSHSP MHI, Katsiveli, May–June 2021: *1* – six-string wave recorder; *2* – acoustic Doppler profiler DVS-6000; *3* – measuring complex Sigma-1; *4* – complex Vostok-M No. 002; *5* – meteorological complex MPV 702.1007; *6* – acoustic Doppler profiler Workhorse Monitor; *7* – stationary oceanographic platform

The Sigma-1 system was sequentially installed at measurement depths ranging from 1 to 7 m at intervals of 0.5–1 m, with each recording lasting 15–20 min. This made it possible to obtain the vertical distribution of the TKE dissipation rate in the upper mixed layer.

Thus, using the downward (W^-) and upward (W^+) velocities recorded in convergence and divergence zones, respectively, the moments at which Langmuir cells passed the measurement system were determined, the dissipation rate was estimated, and the obtained values were related to wind speed and surface wave characteristics using the turbulent Langmuir number La_t [5]. This parameter was calculated using the following relationship:

$$La_t = \sqrt{\frac{u_*}{U_{S0}}},$$

where u_* is the water friction velocity, and U_{S0} is the surface Stokes drift. The Langmuir number characterises the relative influence of wind-induced velocity shear and Stokes-drift shear on boundary layer turbulence. Stokes drift was calculated using the following equation:

$$U_S = A^2 k \omega \exp(-2kz),$$

where A is the wave amplitude; k is the wavenumber; ω is the wave frequency; z is the depth.

During the expeditions carried out in 2021–2024, more than 300 Langmuir cells were identified using records of the vertical current velocity component W; photographic and video materials documenting the sea surface state were collected; the dependence of the downward vertical velocity in convergence zones on wind speed, $W^-(V_{10})$, and the regimes of W^- development at different values of La_t were determined. The intensity of vertical turbulent exchange was estimated using the dissipation rate ε, calculated from the velocity fluctuation spectra according to the method proposed in studies [26, 27].

Results and discussion

Visual observations

A method for observing LC by visualising convergence zones using markers – sheets of paper coated with luminescent paint – was described in [14, 17]. In our experiments, various types of markers were used; wood shavings and sawdust proved to be the most suitable for the spatial scales studied, since they remain on the sea surface longer and form visible bands more quickly. Fig. 3 shows an example of observed Langmuir bands at a wind speed of 10 m/s and a wind direction of 320°; the distance between the bands was 5–8 m. According to our observations, changes in wind speed and direction significantly affect the scale of LC vortices. When the wind speed halved and the wind direction shifted 30° northwards, the distance between the bands decreased to 2–3 m, and their orientation changed (Fig. 3, *b*).

a *b*

F i g. 3. Langmuir bands at the SOP visualised using wood shavings and sawdust: *a* – at 17:53 on 20.08.2024, at V_{10} = 10 m/s; *b* – at 18:57 on 20.08.2024, at V_{10} = 5 m/s

Due to the wide variety of hydrometeorological conditions, our dataset does not yet allow robust statistical relationships between LC vortex sizes and external factors to be determined or the influence of vortex scales on vertical turbulent exchange to be assessed. However, this relationship is qualitatively evident: the conducted experiments demonstrate that the scales of LC and the development of its instability are closely related to changes in wind speed and direction.

Experimental data analysis. LC parameterisation

According to our studies conducted in 2021–2022 [25], LC can intensify near-surface turbulence, with the downward vertical velocity in convergence zones W^- being the most important parameter. It is known that the W^- parameter is related to wind speed. Relationships between W^- and V_{10} previously obtained by other researchers were based on less accurate measurements [17, 18] and a limited amount of observational data.

In our studies, we attempted to refine the relationship $W^-(V_{10})$ by analysing data from the 2021, 2023, and 2024 expeditions. Specialised software was developed in MATLAB for automated data processing and analysis, enabling convergence and divergence zones in LC to be identified from the measured W values. More than 300 Langmuir cells were identified in the analysed dataset at depths of 3–4 m. An example of such a record, with clearly distinguished convergence and divergence zones and characteristic W values, is shown in Fig. 4.

Since the LC system is not stationary but moves to the right of the wind direction, both downward and upward flows pass through the sampling volume of each instrument over time.

Cells for analysis were selected according to the following criteria:

– for a convergence zone: downward velocity W^- from 3 to 60 mm/s; the time taken for the zone to pass the instrument was from 3 to 20 min;

– for a divergence zone: upward velocity W^+ from 2 to 20 mm/s; the time taken for the zone to pass the instrument was from 4 to 40 min.

To determine the stable component of W^- in the convergence zone, the arithmetic mean of all values recorded while the zone passed the instrument was calculated. The same procedure was applied to W^+ in divergence zones.

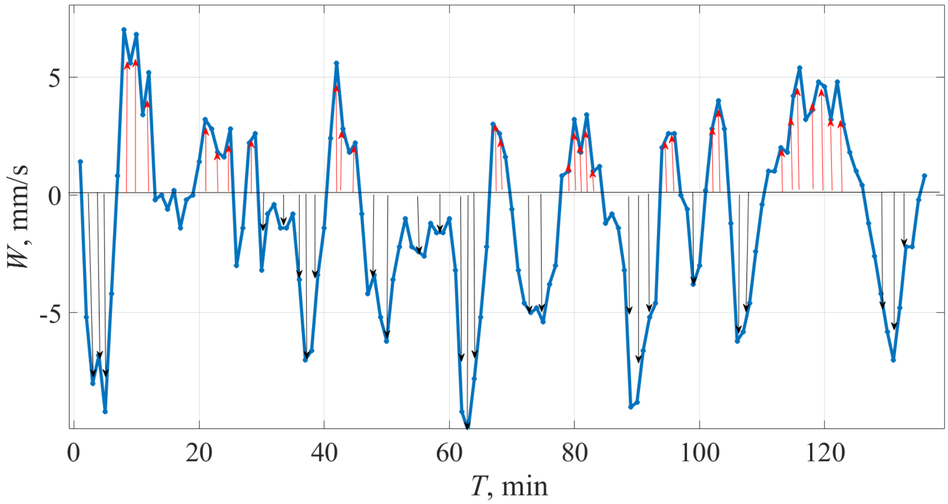

F i g. 4. Convergence (blue arrows) and divergence (red arrows) zones of Langmuir cells identified from measurements of the vertical current velocity component W obtained using the Workhorse Monitor 1200 at a depth of 3 m

The following features were identified during data analysis:

1. Mean W^- values ranged from 3 to 48 mm/s, depending on wind speed.

2. Cells usually passed the instrument in groups of 2–4 over periods of 20–40 min; "nested" cells – small ones inside larger ones – were often observed.

Since the LC system is not stationary but moves to the right of the wind direction, both downward and upward flows pass through the sampling volume of each instrument over time.

Cells for analysis were selected according to the following criteria:

– for a convergence zone: downward velocity W^- from 3 to 60 mm/s; the time taken for the zone to pass the instrument was from 3 to 20 min;

– for a divergence zone: upward velocity W^+ from 2 to 20 mm/s; the time taken for the zone to pass the instrument was from 4 to 40 min.

To determine the stable component of W^- in the convergence zone, the arithmetic mean of all values recorded while the zone passed the instrument was calculated. The same procedure was applied to W^+ in divergence zones.

The following features were identified during data analysis:

1. Mean W^- values ranged from 3 to 48 mm/s, depending on wind speed.

2. Cells usually passed the instrument in groups of 2–4 over periods of 20–40 min; "nested" cells – small ones inside larger ones – were often observed.

To construct the relationship $W(V_{10})$, only mean W^- values in convergence zones were used, as this was a more stable parameter. Hereinafter, W^- is denoted by W for simplicity. The highest-quality records with reliable LC signatures were selected for analysis.

Visual analysis of the $W(V_{10})$ relationship revealed two groups of data demonstrating linear trends. To statistically substantiate this observation, the distribution of W was examined, and its main statistical characteristics were calculated.

The Kolmogorov–Smirnov test (test statistic = 0.285) did not provide grounds for rejecting the hypothesis that *W* was normally distributed at a significance level of 0.05. The mean W_{mean} (5.87 mm/s) and median W_{med} (5.30 mm/s) are close, suggesting that the distribution is relatively symmetric. The standard deviation is 3.02 mm/s, indicating that *W* values predominantly lie between approximately 2.85 to 8.89 mm/s. Values outside this range are less common. Skewness (0.28) is positive but close to zero, indicating a slight right-hand tail (toward higher values). Kurtosis (1.83) is less than 3 (the kurtosis of a normal distribution), indicating that the distribution of *W* is platykurtic relative to a normal distribution.

A comparison between the quantiles of the theoretical normal distribution and the sample quantiles of *W* is shown in Fig. 5.

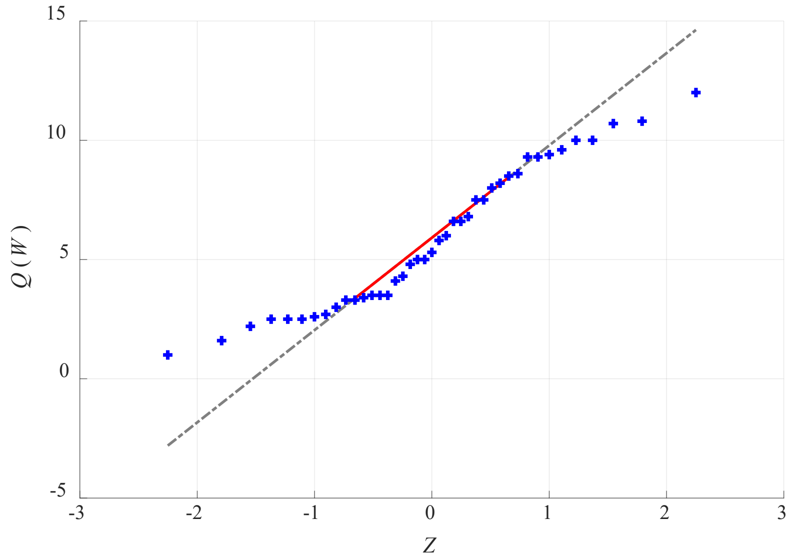

F i g. 5. Comparison of the quantiles of the empirical distribution of *W* ($Q(W)$) with the quantiles of the standard normal distribution (Z). The dashed line $y = x$ corresponds to the theoretical normal distribution; plus signs represent the empirical data, and the red segment indicates the central part of the distribution

Points in the left part of the graph above the reference line indicate that the data contain fewer extremely low values than in the theoretical normal distribution, whereas points in the right part below this line indicate fewer extremely high values. Thus, the distribution of *W* has lighter tails than the normal distribution on both sides.

Based on these results, the following conclusions can be drawn about *W*:

– the distribution of *W* differs slightly from normal and is platykurtic;

– the vertical velocity values lie mainly between 2.85 and 8.89 mm/s, although some values fall outside this range;

– the distribution of vertical velocities is relatively symmetric, with slight positive skewness.

For optimal clustering of the $W(V_{10})$ data, the Gaussian mixture model (GMM) was implemented in MATLAB. The number of clusters was determined using the Akaike information criterion (*AIC*) and the Bayesian information criterion (*BIC*), which allow the optimal number of clusters to be selected by balancing between accuracy and model complexity. The clustering algorithm is as follows:

1. The parameters of the normal distributions of W and V_{10} (means and covariances) and the posterior probabilities of cluster membership are estimated.

2. Based on the *AIC* and *BIC* values, the models with the lowest criterion values are selected (the minima on the ordinate). Fig. 6 shows that the criteria identify two different optimal solutions: four clusters according to the *AIC* and two clusters according to the *BIC*.

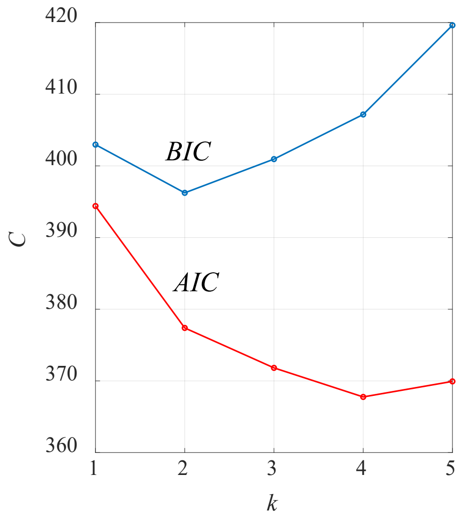

F i g. 6. Dependence of the values of information criteria (*AIC* and *BIC*) C on the number of parameters (clusters) k

In this case, the *BIC* evaluation method offers a more reliable and interpretable model because:

– the *BIC* provides protection against model overfitting by imposing a stronger penalty for model complexity;

– the four-cluster model (selected using the *AIC*) provides the best fit, but is redundant and reflects random variations within the physical regimes rather than the regimes themselves, which complicates its meaningful interpretation;

– the *AIC*-based model is affected not only by the overall patterns of the two regimes but also by random noise and dataset-specific features;

– the two-cluster *BIC*-based model admits a clear physical interpretation and is consistent with the initial visual identification of two regimes presented in the data.

3. After determining the number of clusters, the original V_{10} and W data are divided into groups, and a separate linear model is fitted to each group (Fig. 7).

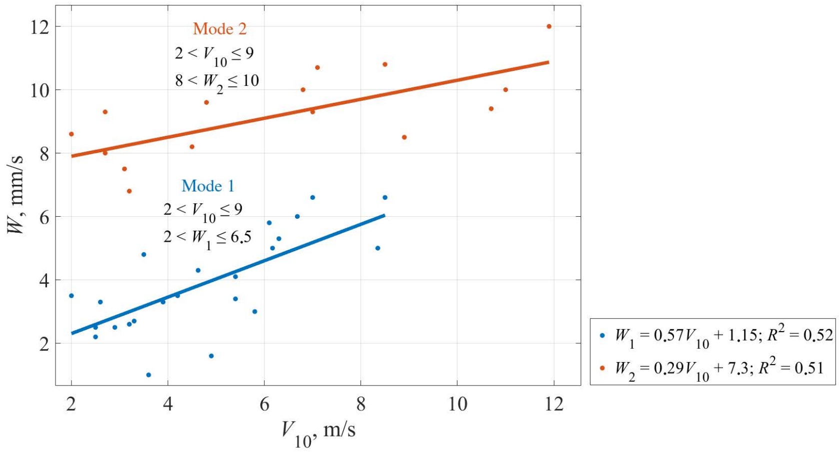

F i g. 7. Data clustering using the GMM method. Dependence of the velocity vertical component (W_1 – for the first mode and W_2 – for the second one) in convergence zones on the average wind speed V_{10}

For each of the two regimes, the vertical velocity component W in convergence zones is approximated as a linear function of wind speed, as follows:

$$W\left(V_{10}\right) = aV_{10} + b,$$

where $a_1 = 0.57 \pm 0.1$ and $b_1 = 1.15 \pm 0.1$ for the first regime, and $a_2 = 0.29 \pm 0.1$ and $b_2 = 7.3 \pm 0.1$for the second regime. The coefficients of determination R^2 are 0.52 and 0.51, respectively. These moderate R^2 values likely reflect the inherent scatter arising from variable hydrometeorological conditions during the experiments.

The first regime is energy-dependent: wind energy is transferred almost entirely to the formation of coherent structures. The steeper slope (0.57) indicates that the vertical velocity component increases with wind speed, reflecting active LC generation. This regime corresponds to the phase of active LC development.

The obtained result is consistent with the Craik–Leibovich theory [28] and the results of numerical modelling, which predict a linear increase in circulation intensity with increasing wind forcing [29], as well as with field measurements showing increasing downwelling velocities with increasing wind speed [30, 31].

The second regime is the "saturated" regime: the system reaches a state where further increases in V_{10} have little effect on W_2 (the small slope coefficient is 0.30). Wind energy is partitioned not into intensifying vertical circulation but into maintaining its maximum intensity and enhancing turbulence. The second regime is implicitly described in the following studies:

– Study [28] showed that there is a balance between LC generation by surface Stokes drift, U_{S0}, and its destruction due to increased turbulence, characterised by the friction velocity u_*. "Saturation" occurs when $La_t \approx 1$, beyond which further wind increases do not strengthen LC but enhance turbulent exchange;

– numerical modeling [29] demonstrates that as La_t increases, the LC kinetic energy initially increases and then approaches an asymptote. The "saturated" regime with a weak dependence on wind speed shown in Fig. 8 corresponds to this asymptotic state.

– field studies [30, 31] using ADCPs and drifters *show* that the measured current velocity components in the convergence and divergence zones of LC do not increase indefinitely with wind speed. Considerable scatter and a tendency to reach maximum values are observed. This behaviour is attributed to interactions with other factors (stratification and wave field), resulting in the saturation effect.

The identified saturation regime, characterised by high W_2 values even at low V_{10} values, suggests that LC intensity is determined not only by instantaneous wind forcing but also by the forcing history and water-column stratification. High W_2 values under weak wind conditions may reflect system inertia associated with the energy of a developed wave field.

To assess the effect of LC on vertical turbulent exchange in the energy-dependent and saturated regimes, we used the parameter La_t. The parameter was calculated directly at the times of the W measurements using synchronous field data on surface waves recorded by a six-string wave recorder. Fig. 8 shows the distribution of La_t for the two identified regimes. Non-overlapping interquartile ranges and the difference between the medians indicate a pronounced difference, suggesting a qualitative change in the structure of turbulence between the regimes.

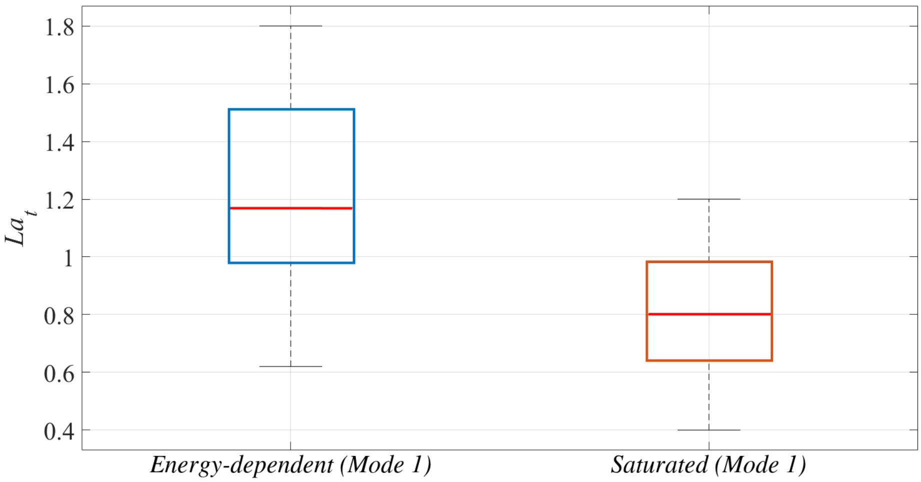

F i g. 8. Distribution of La_t for the energy-dependent and saturated modes of LC. Box plots show medians (red lines), interquartile ranges (box boundaries), and normal value ranges (whiskers)

Effect of LC on vertical turbulent exchange in the wave-enhanced surface layer

As shown in Fig. 8, the energy-dependent regime is characterised by higher La_t values (median 1.2; IQR = 0.53), whereas La_t is lower in the saturated regime (median 0.8; IQR = 0.34). This means that, in the energy-dependent regime, the numerator u_* (water friction velocity) exceeds the denominator U_{S0} (the surface Stokes drift). This indicates that wind-driven shear dominates turbulent exchange while the wave field and Stokes drift remain relatively weak.

In the saturated regime, where La_t is relatively low (≈ 0.8), by contrast, the Stokes drift U_{S0} is larger relative to the friction velocity u_*. This suggests that the wave field is already sufficiently developed and that most of the wind energy is used for wave generation and maintenance (U_{S0} grows faster).

This state may be termed "wave dominance," in which wave processes suppress LC development; this may explain the slow increase in W with increasing wind speed in this regime. The IQR in the energy-dependent regime (0.53) is almost 1.6 times wider than the saturated regime (0.34). This indicates greater variability in the turbulent characteristics in the energy-dependent regime. The smaller scatter in the saturated regime indicates that the system is more stable and remains within a relatively narrow parameter range.

To assess the intensity of vertical turbulent exchange in the wave-enhanced surface layer during the passage of a Langmuir cell through the instrument sampling volumes, the following current velocity fluctuations were recorded: u', v', and w'. The ADCPs and the turbulence meter were separated by approximately 7 m. For each W measurement, seven consecutive five-minute turbulent fluctuation records were selected. The 35-min duration period was assumed sufficient to capture turbulent mixing intensity as a convergence zone passed through the sampling volume. This approach enabled 'scanning' of the turbulence field temporal variability to determine when the ADCP-recorded convergence zone passed through the Sigma-1 sampling volume.

A primary measure of turbulence intensity is dissipation rate ε. Measurements and estimates of ε provide objective information on turbulence intensity, structure, and mixing character. The value of ε was calculated using the method of Stewart and Grant [26], which estimates the dissipation rate from the measured velocity fluctuation spectrum, with minimal contamination from waves and instrument motion.

For each W data point in both regimes (25 points for W_1 and 16 points for W_2), seven ε values were obtained. Thus, 175 values (ε_1) were obtained for the first regime, and 112 values (ε_2) for the second. The mean values and standard deviations of ε for the two regimes were as follows:

1) energy-dependent regime: $(7.04 \pm 14.40) \cdot 10^{-6}$ m^2/s^3;
2) saturated regime: $(4.04 \pm 4.98) \cdot 10^{-6}$ m^2/s^3.

These mean ε values are typical of the sea surface layer under moderate winds and fall within the range of active wind-driven mixing ($\varepsilon \sim 10^{-7}$–10^{-5} m²/s³), which supports their plausibility.

The mean TKE dissipation rate ratio between the energy-dependent and saturated LC regimes is $\varepsilon_1 \approx 1{,}7 \cdot \varepsilon_2$, suggesting differences in turbulence characteristics.

At the same time, the standard deviation σ in the energy-dependent regime ($\pm\, 14.49 \cdot 10^{-6}$) is considerably larger than that in the saturated regime, indicating the highly variable nature of the first regime. This may reflect alternation of periods of active turbulence with periods of relative calm. This is consistent with the larger IQR of La_{t1} in the energy-dependent regime (0.53 vs. 0.34). In the saturated regime, $\sigma = \pm 4.985 \cdot 10^{-6}$ m²/s³ indicates less scatter and suggests that the regime is relatively stable and established; this is also consistent with the smaller IQR of 0.34 for La_{t2}. The turbulent field appears more homogeneous in time and possibly in space.

Within the studied range, no significant linear relationship between ε and W was found for either LC regime ($R < 0.05$). A power-law fit yielded a similarly weak relationship ($R < 0.09$). Analysis of ε IQR between the two regimes confirmed the previously identified differences in turbulence field structure (Fig. 9).

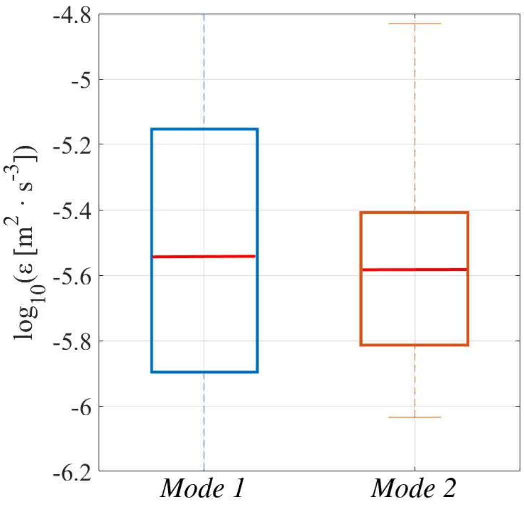

F i g. 9. Distribution of ε for the energy-dependent and saturated modes of LC

The median values of ε_1 and ε_2 are close: $2.87 \cdot 10^{-6}$ and $2.62 \cdot 10^{-6}$ m²/s³, respectively (a difference of ~ 10%). This indicates that the typical dissipation rates at 3 m depth are comparable in both regimes. However, the marked difference in turbulence variability (the scatter in ε_1 and ε_2 values) persists. In the energy-dependent regime, the IQR of ε is $5.76 \cdot 10^{-6}$ m²/s³, which corresponds to IQR of 0.75 on the $\log_{10}(\varepsilon)$ axis. This means that typical ε_1 values can differ by $10^{0,75} \approx 5.6$ times. Such variability indicates pronounced temporal intermittency in the turbulent field, with alternating periods of weak dissipation and intense bursts.

In the saturated regime, the interquartile range is $2.4 \cdot 10^{-6}$ m^2/s^3 ($\log_{10}(\varepsilon)$ *IQR* = 0.40), corresponding to a scatter of ε_2 values by $10^{0.40} \approx 2.5$ times – 2.4 times less than in the energy-dependent regime.

In the saturated regime, established coherent structures organise turbulence into a more stable and predictable dissipation field. Thus, the effect of LC on vertical turbulent exchange in the wave-enhanced surface layer (1–3 m) lies not in altering the mean dissipation rate but in transforming its variability regime – from chaotic and inhomogeneous to more organised and statistically homogeneous.

Conclusion

The characteristics of LC and its effect on vertical turbulent exchange depend not only on wind speed but also on the complex interaction between wind stress and surface Stokes drift. The two identified regimes differ in the development and formation history of LC and thus have different effects on the spatial and temporal distribution of the turbulent field in the sea wave layer.

The existence of two regimes, identified from direct measurements of vertical velocity in convergence zones at the SOP during 2021–2024, is qualitatively consistent with field experiments that estimated LC intensity from indirect indicators: horizontal current divergence and cross-flow amplitude. Unlike previous studies, which were limited to analysing the general wind-turbulence relationship or indirect LC signatures, the present study provides a statistically substantiated distinction between two regimes over the V_{10} range of 2-9 m/s:

– energy-dependent regime ($La_t > 0.98$): $W_1(V_{10}) = 0.57 \cdot V_{10} + 1.15$, with a median La_{t1} of ≈ 1.2 [1.1, 1.5];

– saturated regime ($La_t \le 0.98$): $W_2(V_{10}) = 0.29 \cdot V_{10} + 7.3$, with a median La_{t2} of ≈ 0.8 [0.64, 0.98].

These relationships provide a quantitative parameterisation of the regimes and directly relate them to the turbulent Langmuir number.

Direct measurements analysis of TKE dissipation rate ε at 3 m depth enabled quantitative assessment of the LC effect on turbulent exchange in the sea wave layer. The median dissipation rates in the two identified regimes (energy-dependent and saturated) did not differ significantly: the median values of $\log_{10}(\varepsilon_1)$ and $\log_{10}(\varepsilon_2)$ are −5.541 and −5.582, respectively, corresponding to $\varepsilon \approx 2.87 \cdot 10^{-6}$ and $2.62 \cdot 10^{-6}$ m^2/s^3 (a difference of ~ 10%). The main difference between the regimes lies in TKE dissipation rate variability. In the energy-dependent regime, corresponding to active LC generation, turbulence exhibits pronounced variability: the IQR of $\log_{10}(\varepsilon_1)$ is 0.75, meaning that the typical ε_1 values can vary by a factor of $10^{0.75} \approx 5.6$ across the entire range. For the saturated regime, the IQR of $\log_{10}(\varepsilon_2)$ is 0.40, corresponding to a scatter of $10^{0.4} \approx 2.5$ times across the entire range. Thus, the scatter of ε in the energy-dependent regime is 2.4 times larger than in the saturated one. This indicates the highly variable and intermittent nature of turbulence during the formation of coherent structures in the energy-dependent regime. By contrast, established LC in the saturated regime is associated with more stable turbulent characteristics and substantially lower variability, while the median dissipation rate remains approximately unchanged. These results are consistent with the La_t distribution in both regimes and support the conclusion that the turbulence structure differs fundamentally between them.

For the first time, this study demonstrates that the effect of LC on turbulent exchange in the wave-enhanced surface layer is manifested not as a simple linear $\varepsilon(W)$ relationship but as changes in the statistical properties of the turbulence field. Coherent structures primarily modulate turbulence variability, producing a qualitative transition from a highly variable and inhomogeneous regime to a more organised and statistically homogeneous one, rather than changing the typical dissipation rate. This suggests that the dissipation rate ε is determined by a combination of factors, including stratification, Langmuir cell scale, wind forcing history, and wave field characteristics, and not solely by instantaneous LC intensity. The obtained results provide new insights into the relationship between LC and near-surface turbulence generation and vertical exchange processes.

REFERENCES

1. Craig, P.D. and Banner, M.L., 1994. Modeling Wave-Enhanced Turbulence in the Ocean Surface Layer. *Journal of Physical Oceanography*, 24(12), pp. 2546-2559. https://doi.org/10.1175/1520-0485(1994)024<2546:MWETIT>2.0.CO;2

2. Kudryavtsev, V.N., Shrira, V.I., Dulov, V.A. and Malinovsky, V.V., 2008. On the Vertical Structure of Wind-Driven Sea Currents. *Journal of Physical Oceanography*, 38(10), pp. 2121-2144. https://doi.org/10.1175/2008JPO3883.1

3. Chukharev, A.M., 2013. Multitime Scale Model of Turbulence in the Sea Surface Layer. *Izvestiya, Atmospheric and Oceanic Physics*, 49(4), pp. 439-449. https://doi.org/10.1134/S0001433813040026

4. Craik, A.D.D. and Leibovich, S., 1976. A Rational Model for Langmuir Circulations. *Journal of Fluid Mechanics*, 73(3), pp. 401-426. https://doi.org/10.1017/S0022112076001420

5. Plueddemann, A.J., Smith, J.A., Farmer, D.M., Weller, R.A., Crawford, W.R., Pinkel, R., Vagle, S. and Gnanadesikan, A., 1996. Structure and Variability of Langmuir Circulation during the Surface Waves Processes Program. *Journal of Geophysical Research: Oceans*, 101(C2), pp. 3525-3543. https://doi.org/10.1029/95JC03282

6. Tsai, W.-T. and Hung, L.-P., 2007. Three-Dimensional Modeling of Small-Scale Processes in the Upper Boundary Layer Bounded by a Dynamic Ocean Surface. *Journal of Geophysical Research: Oceans*, 112(C2), C02019. https://doi.org/10.1029/2006JC003686

7. Kukulka, T., Plueddemann, A.J. and Sullivan, P.P., 2012. Nonlocal Transport due to Langmuir Circulation in a Coastal Ocean. *Journal of Geophysical Research: Oceans*, 117(C12), C12007. https://doi.org/10.1029/2012JC008340

8. Li, K., Zhang, Z., Chini, G.P. and Flierl, G.R., 2012. Langmuir Circulation: An Agent for Vertical Restratification? *Journal of Physical Oceanography*, 42(11), pp. 1945-1958. https://doi.org/10.1175/JPO-D-11-0225.1

9. Li, S., Li, M., Gerbi, G.P. and Song, J.-B., 2013. Roles of Breaking Waves and Langmuir Circulation in the Surface Boundary Layer of a Coastal Ocean. *Journal of Geophysical Research: Oceans*, 118(10), pp. 5173-5187. https://doi.org/10.1002/jgrc.20387

10. McWilliams, J.C., Huckle, E., Liang, J.-H. and Sullivan, P.P., 2012. The Wavy Ekman Layer: Langmuir Circulations, Breaking Waves, and Reynolds Stress. *Journal of Physical Oceanography*, 42(11), pp. 1793-1816. https://doi.org/10.1175/JPO-D-12-07.1

11. McWilliams, J.C., Huckle, E., Liang, J.-H. and Sullivan, P.P., 2014. Langmuir Turbulence in Swell. *Journal of Physical Oceanography*, 44(3), pp. 870-890. https://doi.org/10.1175/JPO-D-13-0122.1

12. Sullivan, P.P., Romero, L., McWilliams, J.C. and Melville, W.K., 2012. Transient Evolution of Langmuir Turbulence in Ocean Boundary Layers Driven by Hurricane Winds and Waves. *Journal of Physical Oceanography*, 42(11), pp. 1959-1980. https://doi.org/10.1175/JPO-D-12-025.1

13. Skyllingstad, E.D. and Denbo, D.W., 1995. An Ocean Large-Eddy Simulation of Langmuir Circulations and Convection in the Surface Mixed Layer. *Journal of Geophysical Research: Oceans*, 100(C5), pp. 8501-8522. https://doi.org/10.1029/94JC03202

14. Thorpe, S.A., 2004. Langmuir Circulation. *Annual Review of Fluid Mechanics*, 36, pp. 55-79. https://doi.org/10.1146/annurev.fluid.36.052203.071431

15. Thorpe, S.A., Osborn, T.R., Jackson, J.F.E., Hall, A.J. and Lueck, R.G., 2003. Measurements of Turbulence in the Upper-Ocean Mixing Layer Using Autosub. *Journal of Physical Oceanography*, 33(1), pp. 122-145. https://doi.org/10.1175/1520-0485(2003)033<0122:MOTITU>2.0.CO;2

16. Scully, M.E., Fisher, A.W., Suttles, S.E., Sanford, L.P. and Boicourt, W.C., 2015. Characterization and Modulation of Langmuir Circulation in Chesapeake Bay. *Journal of Physical Oceanography*, 45(10), pp. 2621-2639. https://doi.org/10.1175/JPO-D-14-0239.1

17. Weller, R.A. and Price, J.F., 1988. Langmuir Circulation within the Oceanic Mixed Layer. *Deep Sea Research Part A. Oceanographic Research Papers*, 35(5), pp. 711-747. https://doi.org/10.1016/0198-0149(88)90027-1

18. Filatov, N.N., Rjanzhin, S.V. and Zaycev, L.V., 1981. Investigation of Turbulence and Langmuir Circulation in Lake Ladoga. *Journal of Great Lakes Research*, 7(1), pp. 1-6. https://doi.org/10.1016/S0380-1330(81)72016-1

19. Chukharev, A.M. and Pavlov, M.I., 2021. Model and Experimental Estimates of Vertical Mixing Intensity in the Sea Upper Homogeneous Layer. *Physical Oceanography*, 28(3), pp. 309-325. https://doi.org/10.22449/1573-160X-2021-3-309-325

20. Wu, L., Rutgersson, A. and Sahlée, E., 2015. Upper-Ocean Mixing due to Surface Gravity Waves. *Journal of Geophysical Research: Oceans*, 120(12), pp. 8210-8228. https://doi.org/10.1002/2015JC011329

21. Harcourt, R.R. and D'Asaro, E.A., 2008. Large-Eddy Simulation of Langmuir Turbulence in Pure Wind Seas. *Journal of Physical Oceanography*, 38(7), pp. 1542-1562. https://doi.org/10.1175/2007JPO3842.1

22. Zedel, L. and Farmer, D., 1991. Organized Structures in Subsurface Bubble Clouds: Langmuir Circulation in the Open Ocean. *Journal of Geophysical Research: Oceans*, 96(C5), pp. 8889-8900. https://doi.org/10.1029/91JC00189

23. D'Asaro, E.A., Thomson, J., Shcherbina, A.Y., Harcourt, R.R., Cronin, M.F., Hemer, M.A. and Fox-Kemper, B., 2014. Quantifying Upper Ocean Turbulence Driven by Surface Waves. *Geophysical Research Letters*, 41(1), pp. 102-107. https://doi.org/10.1002/2013GL058193

24. Samodurov, A.S., Dykman, V.Z., Barabash, V.A., Efremov, O.I., Zubov, A.G., Pavlenko, O.I. and Chukharev, A.M., 2005. "Sigma-1" Measuring Complex for the Investigation of Small-Scale Characteristics of Hydrophysical Fields in the Upper Layer of the Sea. *Physical Oceanography*, 15(5), pp. 311-322. https://doi.org/10.1007/s11110-006-0005-1

25. Pavlov, M.I. and Chukharev, A.M., 2023. Influence of Langmuir Circulations on the Intensity of Turbulent Mixing in the Near-Surface Layer of the Sea. In: Karev, V.I., ed., 2023. *Physical and Mathematical Modeling of Earth and Environment Processes-2022*. Cham: Springer, pp. 395-411. https://doi.org/10.1007/978-3-031-25962-3_39

26. Stewart, R.W. and Grant, H.L., 1962. Determination of the Rate of Dissipation of Turbulent Energy near the Sea Surface in the Presence of Waves. *Journal of Geophysical Research*, 67(8), pp. 3177-3180. https://doi.org/10.1029/JZ067i008p03177

27. Soloviev, A., Lukas, R., Hacker, P., Schoeberlein, H., Baker, M. and Arjannikov, A., 1999. A Near-Surface Microstructure Sensor System Used during TOGA COARE. Part II: Turbulence Measurements. *Journal of Atmospheric and Oceanic Technology*, 16(11), pp. 1598-1618. https://doi.org/10.1175/1520-0426(1999)016<1598:ANSMSS>2.0.CO;2

28. Leibovich, S., 1983. The Form and Dynamics of Langmuir Circulations. *Annual Review of Fluid Mechanics*, 15, pp. 391-427. https://doi.org/10.1146/annurev.fl.15.010183.002135

29. McWilliams, J.C., Sullivan, P.P. and Moeng, C.-H., 1997. Langmuir Turbulence in the Ocean. *Journal of Fluid Mechanics*, 334, pp. 1-30. https://doi.org/10.1017/S0022112096004375

30. Smith, J.A., 1992. Observed Growth of Langmuir Circulation. *Journal of Geophysical Research: Oceans*, 97(C4), pp. 5651-5664. https://doi.org/10.1029/91JC03118

31. Gargett, A.E. and Wells, J.R., 2007. Langmuir Turbulence in Shallow Water. Part 1. Observations. *Journal of Fluid Mechanics*, 576, pp. 27-61. https://doi.org/10.1017/S0022112006004575

Submitted 03.03.2026; approved after review 31.03.2026;
accepted for publication 20.05.2026.

About the authors:

Mikhail I. Pavlov, Junior Researcher, Marine Hydrophysical Institute of RAS (2 Kapitanskaya Str., Sevastopol, 299011, Russian Federation), **SPIN-code**: **4194-0706**, **Scopus Author ID**: **57226157217**, **WoS ResearcherID**: **ABB-6151-2021**, **ORCID ID**: **0000-0001-9998-2080**, mixail.pavlov.1993@mail.ru

Alexander M. Chukharev, Leading Researcher, Marine Hydrophysical Institute of RAS (2 Kapitanskaya Str., Sevastopol, 299011, Russian Federation), Head of Basic Department, Sevastopol State University (33 Universitetskaya Str., Sevastopol, 299053, Russian Federation), DSc. (Phys.-Math.), **SPIN-code: 1729-5565**, **Scopus Autor ID: 6603038462**, **WoS ResearcherID: G-3180-2013**, **ORCID ID**: **0000-0003-1078-6425**, alexchukh@mail.ru

Dmitry A. Kazakov, Junior Researcher, Marine Hydrophysical Institute of RAS (2 Kapitanskaya Str., Sevastopol, 299011, Russian Federation), **SPIN-code: 6351-9222**, **Scopus Author ID: 57250141300**, **WoS ResearcherID: ABB-9621-2021**, **ORCID ID: 0000-0001-5083-4968**, dk@mhi-ras.ru

Anatoly G. Zubov, Junior Researcher, Marine Hydrophysical Institute of RAS (2 Kapitanskaya Str., Sevastopol, 299011, Russian Federation), **Scopus Author ID:** 57215362329, sl4612@mail.ru

Olga I. Pavlenko, Leading Software Engineer, Marine Hydrophysical Institute of RAS (2 Kapitanskaya Str., Sevastopol, 299011, Russian Federation), **Scopus Author ID**: 57215363083, olpav@list.ru

Sergey A. Shutov, Leading Engineer, Marine Hydrophysical Institute of RAS (2 Kapitanskaya Str., Sevastopol, 299011, Russian Federation), sergeo808@gmail.com

Contribution of the co-authors:

Mikhail I. Pavlov – conceptualization, data curation, methodology, investigation, writing – original draft preparation, review and editing

Alexander M. Chukharev – data curation, project administration, writing – review and editing

Dmitry A. Kazakov – investigation of the research data

Anatoly G. Zubov – investigation of the research data

Olga I. Pavlenko – data curation, formal analysis, validation of the results

Sergey A. Shutov – investigation of the research data

The authors have read and approved the final manuscript.
The authors declare that they have no conflict of interest.